Surface trap mediated electronic transport in biofunctionalized silicon nanowires

F Puppo[1,3], F L Traversa[2], M Di Ventra[2], G De Micheli[1] and S Carrara[1]

[1] Integrated Systems Laboratory, École Polytechnique Fédérale de Lausanne, Lausanne 1015, Switzerland
[2] Department of Physics, University of California, San Diego, La Jolla, CA 92093, USA

E-mail: francesca.puppo@epfl.ch, ftraversa@physics.ucsd.edu, diventra@physics.ucsd.edu, giovanni.demicheli@epfl.ch and sandro.carrara@epfl.ch

CrossMark

Abstract

Silicon nanowires (SiNWs), fabricated via a top-down approach and then functionalized with biological probes, are used for electrically-based sensing of breast tumor markers. The SiNWs, featuring memristive-like behavior in bare conditions, show, in the presence of biomarkers, modified hysteresis and, more importantly, a voltage memory component, namely a voltage gap. The voltage gap is demonstrated to be a novel and powerful parameter of detection thanks to its high-resolution dependence on charges in proximity of the wire. This unique approach of sensing has never been studied and adopted before. Here, we propose a physical model of the surface electronic transport in Schottky barrier SiNW biosensors, aiming at reproducing and understanding the voltage gap based behavior. The implemented model describes well the experimental I–V characteristics of the device. It also links the modification of the voltage gap to the changing concentration of antigens by showing the decrease of this parameter in response to increasing concentrations of the molecules that are detected with femtomolar resolution in real human samples. Both experiments and simulations highlight the predominant role of the dynamic recombination of the nanowire surface states, with the incoming external charges from bio-species, in the appearance and modification of the voltage gap. Finally, thanks to its compactness, and strict correlation with the physics of the nanodevice, this model can be used to describe and predict the I–V characteristics in other nanostructured devices, for different than antibody-based sensing as well as electronic applications.

S Online supplementary data available from stacks.iop.org/nano/27/345503/mmedia

Keywords: silicon nanowire, surface state, analytical model, voltage gap, memristive biosensor, tumor extract, biomarker

(Some figures may appear in colour only in the online journal)

1. Introduction

The formation of surface dangling bonds is a very well-known phenomenon in silicon device technology. The most common techniques for the fabrication of silicon nanowires (SiNWs) are based on the top-down approach. Top-down fabricated devices rely on lithographic patterning to produce the nanoscale structure, typically by etching. While electron-beam lithography (EBL) leads to the high-resolution definition of nanostructured devices, chemically-assisted etching processes are very aggressive, and result in surface roughness and silicon surface defects [1]. Surface defects are usually associated with dangling bonds defined by missing Si crystal atoms at the surface that leave unsaturated bonds behind them [2]. These unsaturated bonds at the surface give rise to

allowed energy states within the forbidden energy gap that are referred to as surface states [3].

Hysteresis in the electrical characteristic of nano-electronic devices, such as carbon nanotubes (CNTs) [4–6] or SiNWs [7, 8], is one of the first indications of the presence of surface traps. Recently, Schottky barrier SiNWs with controlled hysteretic features have been fabricated and used for high-sensitive detection of biomolecules after their functionalization with antibodies [9]. Experimental measurements demonstrated that our SiNW based sensors show a peculiar behavior that is reminiscent of complex memristive and memcapacitive effects, namely resistive and capacitive effects with memory [10–12], when charged species come into contact with their surface. Charged molecules from the surrounding environment determine a sort of memory effect in terms of voltage that has been denoted as voltage gap [13]. Specifically, the voltage gap is defined as the voltage difference between the two current minima in the semi-logarithmic *I–V* curve of the hysteretic device. It depends on the net charge brought by the molecules to the nanowire surface, thus enabling the sensing of varying concentrations of chemical and biological species [9, 14]. This new class of biosensors based on memristive SiNWs, functionalized with biomolecules, and focused on voltage gap changes as a detection transduction method, takes the name of memristive biosensors [13]. On the other hand, SiNW field-effect transistor (SiNW-FET) sensing techniques, based on electrical measurement of the device conductance as a function of ion or biomolecule concentrations, has been mostly adopted and investigated for biodetection, mainly in an ideal environment, i.e. phosphate buffered saline solution (PBS) [15–20].

In this paper we propose a voltage gap approach with nano-fabricated devices as an alternative detection technique [9, 13, 14]. The experimental data show that this novel sensing method has the potential to overcome the main limitations of low sensitivity in real human samples, such as a tumor extract (TE), with SiNW-FET based sensors [21, 22], thanks to both the increased detection robustness of the voltage gap parameter and the enhanced sensitivity due to another novelty dealing with measurement in air [23], which aims at increasing the Debye screening length [24, 25].

2. Experiments

The SiNWs employed for this work were fabricated on SOI wafer using a top-down process based on a deep reactive ion etching (DRIE) technique described in the experimental section of the supporting information (SI). The scanning electron microscopy (SEM) characterization of the fabricated structures is given in figure 1. Figure 1(a) illustrates the top-view image of a device having a nanowire channel 420 nm long and 35 nm wide. Figure 1(b) shows the tilted-view of the same and shows the vertical stack of nanowires. The nanoscale structures bridge source and drain NiSi contacts that are highlighted in green in both figures for correspondence with the schematic design reported in the SI.
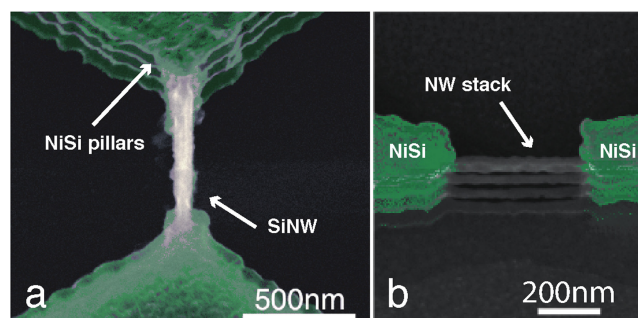

Figure 1. SEM images of a fabricated memristive SiNW device bridging two NiSi contact pads. (a) Top-view SEM image; (b) tilted-view image showing the vertical stack of nanowires.
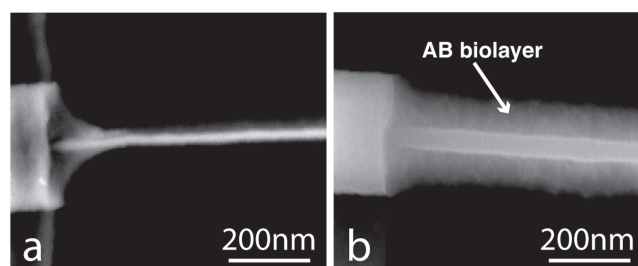

Figure 2. SEM images of a fabricated memristive SiNW (a) before and (b) after the surface biomodification process.

A specific antibody (AB) was linked to the native oxide of the device by means of silane chemistry [26] to functionalize the SiNW, and blocking agents [27] were used to improve the surface specificity of the sensor. Both protocols for surface biofunctionalization and antigen (AG) sensing are described in detail in the experimental section of the SI.

Characterization of the biofunctionalization process was performed both by observation with SEM and fluorescence imaging. In figure 2 we report the SEM micrographs of one of the fabricated devices (a) before and (b) after surface biomodification. From figure 2(b) it is clearly evident the formation of a biolayer of AB around the nanostructure. Figure 3(a) shows the semi-logarithmic I_{ds}–V_{ds} curve of one fabricated SiNW device. The I_{ds}–V_{ds} curve presents a hysteresis loop that is pinched at $V_{ds} = 0$ V for devices with bare surfaces (black curve), and is clear mark of a memristive system [10, 11]. Once functionalized with ABs, the *I–V* curve of the sensor changes (figure 3(a)); a non-zero current is now observed when the voltage is swept back to zero (red curve), which is different from the initial condition of zero current at zero voltage. The pinched loop is lost and replaced by a voltage gap defined by the difference in voltage between the crossing points of the forward and backward V_{ds} curves with the *x*-axis. When the sensor is exposed to a solution of specific AG, then washed, dried and measured, a shrinking of the voltage gap is clearly visible. This shrinking is dependent on the concentration of the target molecule, as demonstrated by the calibration curve reported in figures 3(b) and (c). Details on the sensing protocol and the electrical acquisition are reported in section I of the SI. It is important to observe that all the measurements are performed in air, under fixed relative
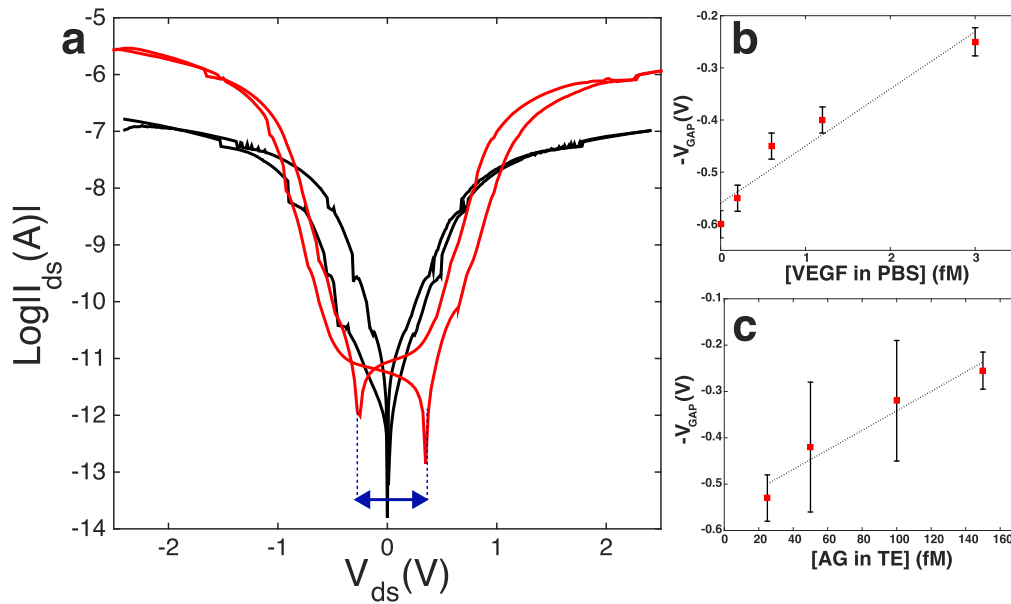
Figure 3. The voltage gap detection approach. (a) The fully pinched hysteresis loop of a just fabricated SiNW (black curve) is lost when its surface is modified with AB (red curve). The adsorption of charged proteins is demonstrated by the augmented current peak and the appearance of a voltage gap. The voltage gap is a parameter of sensing; it decreases as a function of femtomolar concentrations of vascular factors in PBS (b), and as a result of the sensing of AG in the more challenging environment of a breast TE (c). The reported error bars stand for the standard deviation of multiple measures of the same sensor (b), and the standard deviation of the voltage gap acquisitions are related to three similar devices under the same exposure conditions (c).

humidity conditions [9] that are kept constant by continuous monitoring in a sealed measurement chamber. This set-up avoids contamination and creates stable conditions for repeatability of the experiment. Note that a number of control experiments are performed with the aim of defining the electrical noise introduced by interfering species. For example, the effect of silanization on the voltage gap variation has been acquired and, by comparison, estimated to be negligible with respect to the voltage gap modification measured after AB functionalization and AG uptake. Testing the effect of the blocking step with gelatin would lead to further information on the charge-based behavior of the AB–AG complex. In figure 3(b) the experiment consisted of in-air sensing, with the voltage gap technique, of the cancer marker vascular endothelial growth factor (VEGF), diluted in PBS solution in very low concentrations (fM). Figure 3(c) reports the most recent results achieved in the detection of small amount (75–150 fM) of rabbit AG dispersed in the more challenging environment of a breast TE. The TE is prepared directly from patient biopsies (see the SI for details on the TE preparation process), with formation of a cell lysate that is then used for sensing once diluted in PBS, without any kind of filtering. The final concentration of the detected AG in the TE is extremely challenging considering the 100 000 fold mass excess of nonspecific tumor proteins. Data illustrated in figure 3(c) demonstrate the capability of this novel technique in profiling very small concentration changes after interaction with a real biological sample. To the best of our knowledge, the literature reports very few works on immuno-biosensors based on SiNWs capable of measuring femtomoles of AGs in a complex sample such as a TE. Most of the high-sensitive results have been achieved with SiNW-FETs for the detection of

RNA with DNA based probes [28]. Very recently, SiNW-FET based in-air immuno-biosensors have been demonstrated as a valid candidate for the highly sensitive detection of cancer markers in real patient samples [23]. However, these results are based on the electrical measurement of the conductance according to the state-of-the-art ISFET technology. In this article we intend to report, for the very first time, an interesting alternative to the femtomolar detection in real breast TEs with memristive immuno-based SiNWs. Memristive nanowires have already been proposed for memory and computation applications but never as ultra-highly sensitive biosensors for detection in breast tumor tissues.

It is important to observe that the voltage gap strictly depends on the sign of charges carried by molecules from the surrounding environment. Typically, the charge-based behavior of molecular species such as proteins can be predicted by considering their isoelectric point (pI) and by comparing it to the pH conditions of their surrounding liquid matrix. However, when dealing with polyclonal ABs, such as in the case of the present work, the definition of their pI can be very complex. Indeed, polyclonal ABs have no set pI because they are mixtures of various immunoglobulin classes that can alter their net charge and electrical behavior depending on the measurement conditions. Although this complicates the situation, a number of scientific observations have helped to infer the predominant charge-based behavior of the molecules used. Experimental evidence has demonstrated that molecular species carrying a positive net charge are responsible for the appearance and increase of the voltage gap parameter in the I_{ds}–V_{ds} characteristic of the memristive device. On the other hand, species having opposite, negative charge have shown the compensation of this effect by decreasing the voltage gap.

Carrara *et al* have shown that the effect observed in bio-functionalized memristive devices is equivalent to the one of nanostructures without any biofunctionalization, but fabricated with an all-around silicon gate [13]. A positive bias applied to the all-around gate defines an increased voltage gap with respect to the negative one that leads instead to its reduction [29]. This was found to be in agreement with the observation that the ABs, under the correct physiological conditions (pH 7.4), contribute to a positive net charge all around the nanowire because of the slight majority of arginine and lysine residues carrying positive charges [13]. Further experimentation has demonstrated that increasing concentrations of positively charged ions in solution lead to an enlarged voltage gap, such as in the case of Na^+ [14] or ammonium (NH_4^+) ions (data not reported here). Moreover, considering that the AG molecule interacts and binds with its specific AB receptor by electrostatic interactions, such as var der Waals forces, it is reasonable to think that the target AG species bring to the surface of the device charges of opposite sign with respect to the AB, i.e. an imbalance of negative charge that compensates for the positive voltage gap increase. A further confirmation of our charge-based schema can be found by considering similar experiments performed by the authors with SiNW-FETs [23, 30]. Here, the conductance increases for detection of negatively charged AGs with p-type SiNW-FETs in accordance with the ISFET theory.

Despite available data showing the achievement of high-specific and sensitive biosensing using the voltage gap approach, both in ideal (figure 3(b)) and real conditions (figure 3(c)), a deeper theoretical study on the physical meaning of the voltage gap in nano-electronic devices, as well as its dependence on external charges from biomaterials, is still missing. Here, we propose a physics-based compact model that describes very well the occurrence of the voltage gap in biomodified Shottky barrier SiNWs, and links this effect to the interaction of charged species with the surface of the wires. Thanks to its evident correlation with the physics of the device, the model could also be used to make predictions, and be included in commercial circuit simulators, such as SPICE [31].

3. Model

The voltage gap based sensors display a complex electrical behavior that is the result of the particular nanoscale structure of the device. The experimental data demonstrate that the hysteretic behavior of the sensor is strongly dependent on the variation of the surrounding environment, such as the temperature [32], the humidity [9], charges from dissolved ions in solution [14], and functionalization with biomolecules [9]. These observations suggest that voltage gap based sensing is mostly based on the phenomenon of charge imbalance at the surface of the device, where charge traps continuously change their state if solicited by an external bias and modified through exposure of the surface dangling bonds to different concentrations of biomarkers. Moreover, the fabricated nanostructures have nickel silicide (NiSi) Schottky barriers.

Considering the work of Sacchetto *et al* [13, 29], as well as the experimental results, we argue that the effects at the NiSi/SiNW junctions also affect the memristive behavior of our nanostructures, and the variation of the voltage gap as a function of molecular species at their surface.

Starting from these hypotheses, we model the voltage gap based sensor as a combination of multiple interacting transport mechanisms: (i) the transport through the surface states ($I_{\text{drift}}^{\text{ox}}$, $I_{\text{diff}}^{\text{ox}}$), (ii) the transport in the bulk of the SiNW (I^{NW}), and (iii) the transport at the Schottky junctions across the two potentials V_1 and V_2. Each of them is represented by a different circuit element in the equivalent circuit sketched in figure 4.

The fabricated structures are characterized by a p-doped nanoscale channel (35 nm) with surface roughness and defects. Surface defects can give rise to energetically active surface states continuously distributed in energy within the silicon band-gap [3, 33, 34]. Their charge state is Fermi-level dependent [35], thus defining the amphoteric nature of the surface traps. Depending on the position of the semiconductor Fermi level with respect to the charge neutrality level (namely the level at which surface charges are compensated by the bulk doping atoms), the surface states can act either as electron acceptors or electron donors, being associated with either acceptor-like or donor-like energy levels, respectively [36]. Figure 5 illustrates a possible schematic model of the surface of a SiNW with native oxide and surface trap centers, where surface state recombination occurs due to the adsorption of external molecules such as ABs.

All the transport mechanisms we deal with at the surface can be subdivided into drift and diffusion components [37–39]. We describe in detail each of them separately.

Current components from surface states. In the most simplified approximation, the drift component of donor-like and acceptor-like surface trap centers can be described by resistor–capacitor (RC) networks [39] acting independently when a voltage is applied across them (figure 4). The overall effect arising from the activity at the acceptor (donor) sites is reduced to an equivalent resistance R_{a} (R_{d}) in parallel to an equivalent capacitance C_{a} (C_{d}). In first approximation, and for short wires, the electrical capacitances of acceptor and donor RC networks can be assumed proportional to the number of acceptor, n_{a}, and donor, n_{d} charges, respectively, because they act as parallel capacitances associated with their respective charges. If $n_{\text{a}}(t)$, $n_{\text{d}}(t)$ and $n_{\text{n}}(t)$ denote the time dependent amount of acceptor-like (negatively charged), donor-like (positively charged) and neutral traps, respectively, the total number of charge states N_0 can be expressed as:

$$N_0 = n_{\text{a}}(t) + n_{\text{d}}(t) + n_{\text{n}}(t). \quad (1)$$

Therefore, the various capacitances can be defined as:

$$C_\alpha = \tilde{C}_\alpha \frac{n_\alpha(t)}{N_0} \quad (2)$$

where $\alpha = $ a, d (acceptor, donor), $\tilde{C}_\alpha$ is the overall capacitance of the trap systems, and the initial condition for the n_α are discussed in section III of the SI. The equivalent resistances of surface charged centers, R_α, with $\alpha = $ a, d can
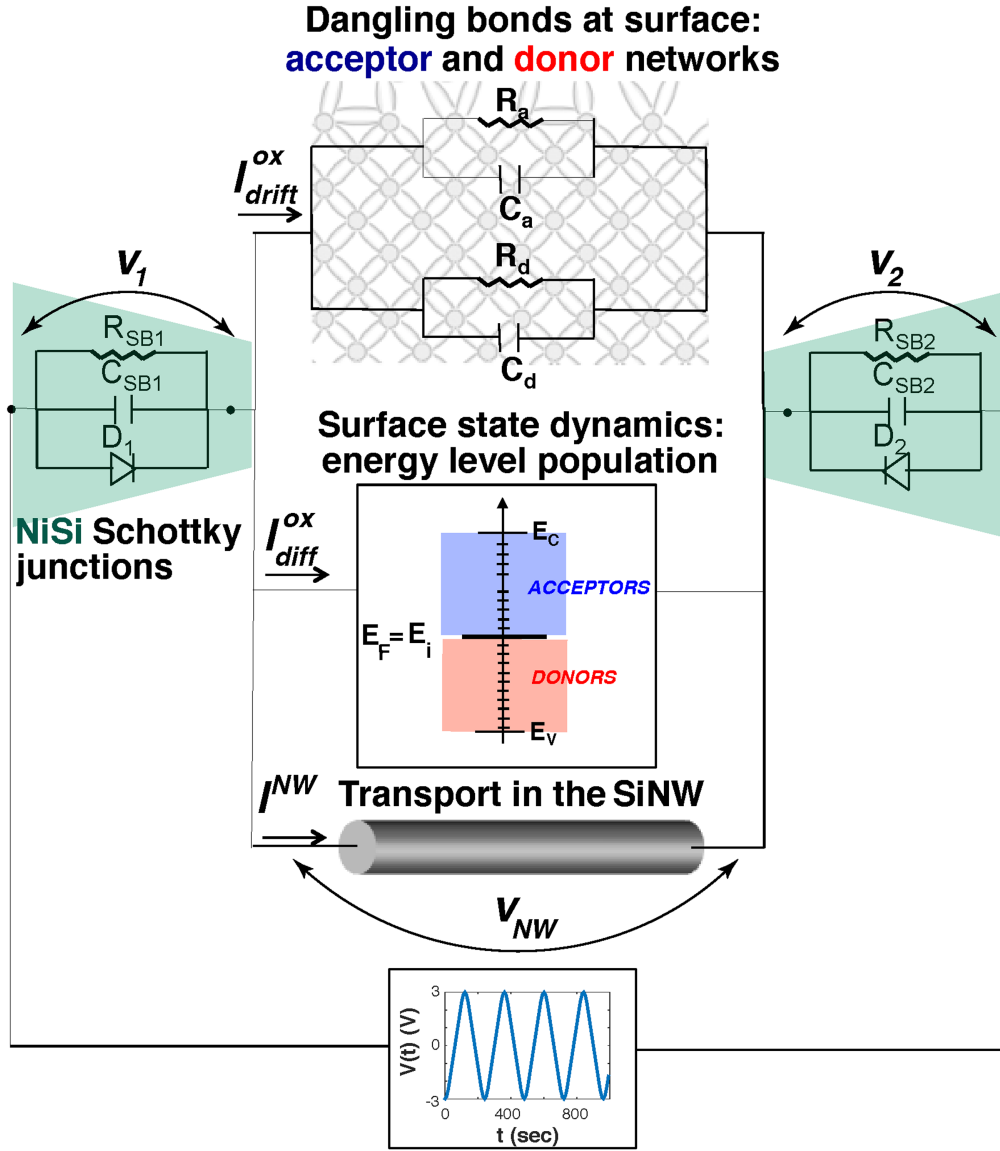
Figure 4. Equivalent circuit representing the multiple transport mechanisms in SiNW.

be estimated by means of the Einstein relation [40], and expressed as:

$$R_\alpha = \left[\frac{q n_\alpha \mu_\alpha}{L} A e^{\frac{\Delta E}{k_B T}} \right]^{-1} \qquad (3)$$

where q is the electric charge of a particle, μ_α stands for the electrical mobilities of the charged traps, A is the transport area, k_B is the Boltzmann constant, T the absolute temperature, and ΔE the free energy change for surface traps to vary their states [40].

Using relations (2) and (3) the drift surface current $I_{\text{drift}}^{\text{ox}}$, driven by the external voltage bias $V(t)$, and due to the impedance of the RC network, is created by the hopping of charges from one surface trap to another and reads:

$$I_{\text{drift}}^{\text{ox}}(t) = \frac{R_a + R_d}{R_a R_d} V_{\text{NW}}(t) + \frac{d}{dt}[(C_a + C_d) V_{\text{NW}}], \qquad (4)$$

where V_{NW} is the voltage drop across the nanowire channel (see figure 4).

The second contribution to the surface current is given by the diffusion current $I_{\text{diff}}^{\text{ox}}$. The diffusion process is due to the concentration gradient of charged surface states. From the current continuity equation, following the approximation described in [39], and also discussed in section II of the SI, we have

$$I_{\text{diff}}^{\text{ox}} = e \left(-f_a \frac{dn_a(t)}{dt} + f_d \frac{dn_d(t)}{dt} \right), \qquad (5)$$

where f_a and f_d are self-similarity parameters (see SI for the definition) to be fitted to the experimental data, and e the electron charge.

Assuming that no mixing of acceptor-like and donor-like states occurs at low frequency we can approximate the recombination/formation rate of the surface traps $n_a(t)$ and $n_d(t)$ as a linear function of the surface state densities:

$$\frac{dn_\alpha}{dt} = -k_\alpha^\alpha(V_{\text{NW}}) n_a + k_n^\alpha(V_{\text{NW}}) n_n \qquad (6)$$
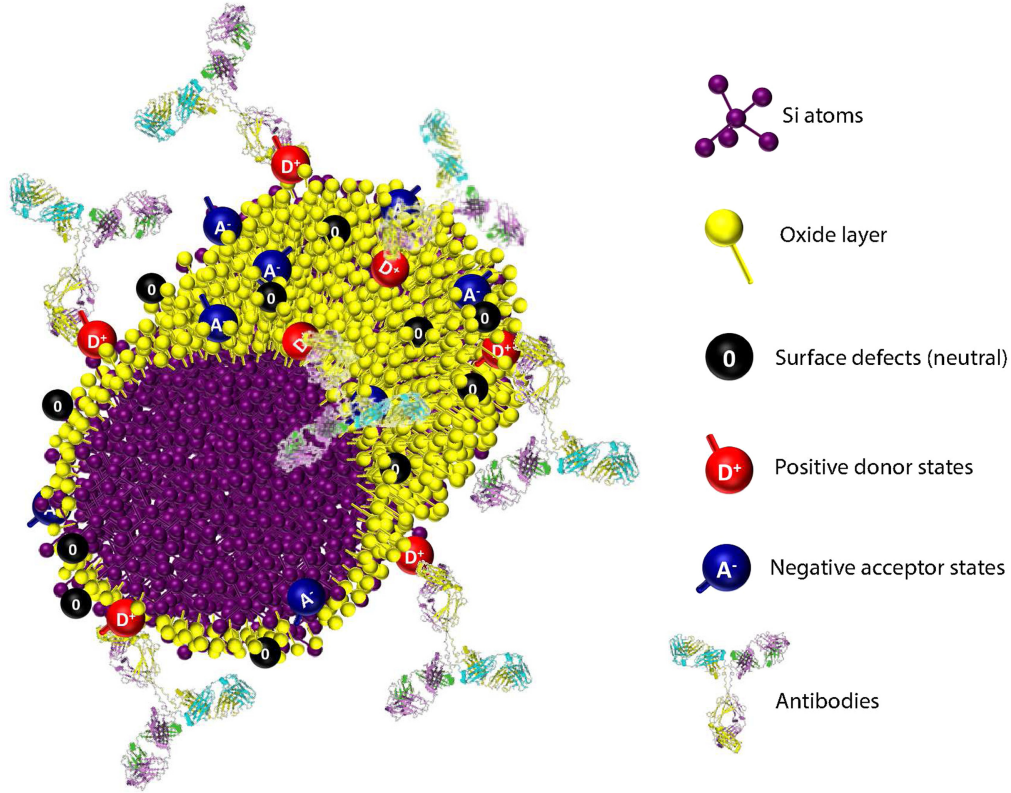
Figure 5. Sketch of the formation/recombination of energetic surface levels. Neutral (black spheres), acceptor-like (blues spheres) and donor-like (red spheres) states are from surface defects. Charging phenomena at the surface take place via binding of charged species such as ABs.

where $\alpha = $ a, d, and k_d^d, k_a^a and k_n^α denote the charge acceptor, donor and neutral rate constants, respectively. The first term on the r.h.s. of equation (6) represents the inter-band hopping of charge species α from its band to the neutral band (state recombination), while the second term represents the reverse process (state formation). These rate constants are estimated using the modified Arrhenius rate equations [39]:

$$k_\alpha^\alpha(V_{NW}) = k_{\alpha 0}^\alpha e^{\frac{-\beta_\alpha(E_\alpha^\alpha - eV_{NW})}{\sigma T}},$$
$$k_n^\alpha(V_{NW}) = k_{n0}^\alpha e^{\frac{(1-\beta_\alpha)(E_n^\alpha - eV_{NW})}{\sigma T}} \tag{7}$$

with k_{a0}^a, k_{n0}^a and k_{d0}^d, k_{n0}^d the rate constants of acceptor and donor traps in their charged or neutral state, respectively, applicable when $V(t) = 0$. Moreover, $k_{\beta,0}^\alpha$ is not independent among them and its dependence is discussed in section III of the SI. E_β^α is the average energy for the inter-band formation/recombination processes (see SI for the continuum to discrete energy band approximation). β_a and β_d represent the symmetrization factors; σ describes the response of the rate constants to the external voltage due to multiple scatterings.

Current components from the SiNW bulk. The electronic transport in the bulk of the SiNW is described by drift I_{drift}^{NW} and diffusion I_{diff}^{NW} components. I_{drift}^{NW} can be expressed as a function of the wire resistance R_{Si} and voltage drop V_{NW} across it:

$$I_{drift}^{NW} = \frac{V_{NW}}{R_{Si}} \tag{8}$$

where R_{Si} is estimated as $\rho_{p-Si}\frac{L}{A}$, with ρ_{p-Si} the resistivity of low (10^{15} cm^{-3}) boron doped silicon (5M Ω cm), and L and A the length and the cross section area of the wire, respectively.

The diffusion component I_{diff}^{NW} depends on the concentration gradient of the net charge into the nanowire. In this case, we can estimate the total net charge in the bulk as the sum of the net charges Q_1 and Q_2 at the depletion regions induced by the Schottky contacts. Using again the approximation in section III of the SI, the diffusion current in the wire can be thus estimated as:

$$I_{diff}^{NW} = -f_s \frac{d(Q_1 + Q_2)}{dt} \tag{9}$$

with f_s a self-similarity coefficient resulting from the continuity equation approximation (see section II of the SI). The net charges Q_1 and Q_2 can be evaluated using the standard expression for depletion region net charge [37] $Q_j = -SN_dw_{dj}$ where $j = 1, 2$, S is the section area of the junctions and N_d the number of ionized donors of the p-type SiNW. w_{d1} and w_{d2} are the thicknesses of the left and right depletion regions formed by the Schottky junctions at the source and drain terminals and can be estimated as [37] $w_{dj} = \sqrt{2\epsilon_0\epsilon_s(\phi_{bi} - V_j)/qN_d}$ with ϕ_{bi} the built-in potential of the NiSi/Si junction, and V_1 and V_2 the voltage across the left and right Schottky barriers, respectively.

Current components from the Schottky contact. The last factor affecting the electrical behavior of the voltage gap based sensor is the metal–semiconductor interface. The NiSi Schottky barriers can be modeled as different elements in
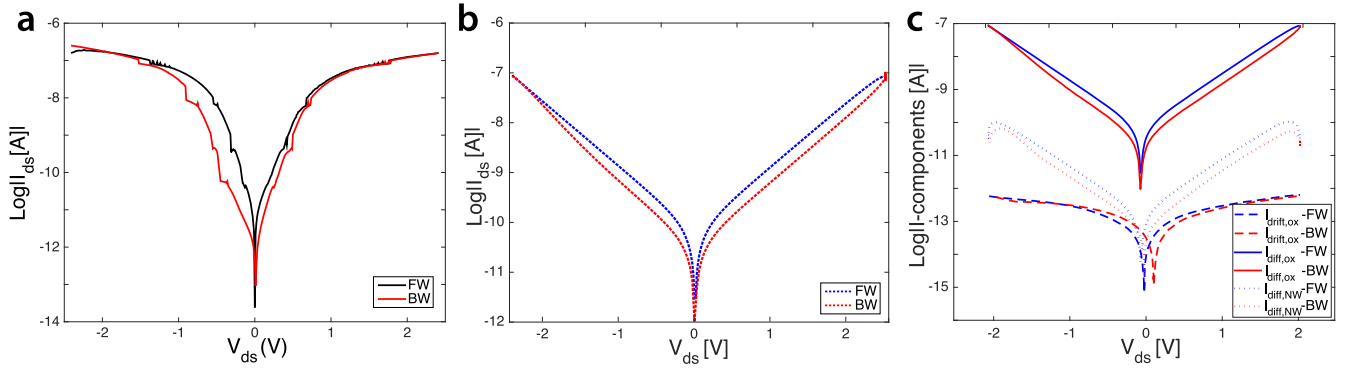
Figure 6. Experimental (a) and simulated (b) I_{ds}–V_{ds} characteristics of a SiNW before any surface biomodification. Both curves have pinched hysteresis loops, similar to the hysteresis of memristive-like behavior, and same current peak. Blue and red curves denote the forward and backward current branches, respectively. (c) Corresponding components of the total current reported in (b). The parameters chosen for this simulation are: $k_{a0}^a = 3.5 \times 10^{-4}$ Hz, $k_{n0}^a = k_{a0}^a/[8.4(N_0 - n_{d,0})/n_{d,0}]$, $k_{n0}^d = 2 \times 10^{-4}$ Hz, $k_{d0}^d = (N_0 - n_{d,0})/n_{d,0} \times k_{n0}^d$, $\tilde{C}_a \sim \tilde{C}_d = 10^{-12}$ F, $R_a = 10^3$ MΩ, $R_d = 10^6$ MΩ, $\sigma = 6.5$, $\beta_a = \beta_d = 1/2$, $f_a = 2.8 \times 10^{14}$, $f_d = 3 \times 10^{10}$, $f_s = 2 \times 10^{16}$, $\Delta E = 253$ eV, $n_d/N_0 = 0.01$, $N_0 = 8.5$.

parallel (figure 4): the resistance R_{SB1} (R_{SB2}), capacitance C_{SB1} (C_{SB2}), and the diode $D1$ ($D2$) define the left (right) NiSi Schottky barrier of the nanowire. From the equivalent circuit, it derives that the current flowing through the left and right Schottky barriers is expressed as:

$$I_{SBj} = C_{SBj}\frac{dV_j}{dt} + \frac{V_j}{R_{SBj}} + I_{Sj}(e^{\frac{qV_j}{k_BT}} - 1) \qquad (10)$$

with $j = 1, 2$. I_{S1} and I_{S2} are the saturation currents of the left and right diodes and are defined by [38] $I_{Sj} = A^{**}T^2S \exp[-q\phi_{bi}/k_BT]$ with A^{**} the Richardson's constant and ϕ_{bi} the built-in potential of the NiSi/Si junction. The resistances of the Schottky diodes R_{SB1} and R_{SB2} can be estimated by the contact-resistance relationship [37] $R_c = \frac{k_B}{A^{**}Tq}e^{[q\phi_{bi}/k_BT]}$. The Schottky diode capacitances C_{SB1} and C_{SB2} are expressed by the diode capacitance–voltage relationship [41] $C_j = C_{j0}(1 - V_j/\phi_{bi})^{-\gamma}$, where C_{j0} is the zero-bias junction capacitance and γ is a parameter representing the doping profile of the active junction layer ($\gamma = 0.5$ for a uniformly doped junction layer). The zero-bias junction capacitance is $C_{j0} = S\epsilon_0\epsilon_r/w_d$ with ϵ_0 and ϵ_s the vacuum dielectric constant and the relative permittivity of the silicon, respectively.

Dopant atoms introduced into semiconductors are known to have the effect of varying the effective barrier height in a given metal–semiconductor contact [37, 38]. Surface charges have a similar effect on the junctions of our device and induce a Schottky barrier lowering $\phi_{bi} - \Delta\phi_{bi}$. The image-force lowering, also known as the Schottky effect or Schottky barrier lowering, is the image-force-induced lowering of the barrier energy for charge carrier emission, in the presence of an electric field. The charge carriers in our case are represented by the charges related to the surface distribution of acceptor and donor trap states. The barrier lowering is estimated by considering the image-force lowering theory [37] $\Delta\phi_{bi} = \frac{q^3 n_s \psi_s}{8\pi^2(\epsilon_r\epsilon_0)^3}$ where n_s is the charge volume density given by the sum of the net surface charge volume density $\frac{n_d - n_a}{\text{Volume}}$, the bulk doping atoms N_d, and ψ_s the surface potential. The

barrier lowering affects the Schottky barriers by changing the saturation currents with two terms related to the different effects of positive (donors) and negative (acceptors) mobile charge carriers at the Schottky barriers: positive carriers see a barrier height $\phi_{bi} - \Delta\phi_{bi}$, while negative carriers see a barrier $E_{Si,gap} - \phi_{bi} - \Delta\phi_{bi}$ where $E_{Si,gap}$ is the silicon energy band-gap:

$$I_{S,j} = A^{**}T^2S\left(e^{-\frac{q(\phi_{bi} - \Delta\phi_{bi})}{k_BT}} + e^{-\frac{q(E_{Si,gap} - \phi_{bi} + \Delta\phi_{bi})}{k_BT}}\right) \qquad (11)$$

4. Results and discussion

By combining all the analytical formulations reported in the previous section, the circuit of figure 4 can be solved for a varying external voltage. The phenomena at the SiNW surface, in the bulk, and at the Schottky barriers can be expressed by a system of differential equations in the four variables $V_1(t)$, $V_2(t)$, $n_a(t)$ and $n_d(t)$. This system describes the dynamic interaction of the nanodevice with the incoming molecules, and its solution defines the current–voltage relation, enabling the comparison with the electrical characteristics acquired during the experiments. The analytical formulation of the circuit was implemented in Matlab, and the solution was calculated throughout an implicit numerical solver endowed with time step size control programmed ad hoc for this particular problem.

The external bias voltage is swept from −2.5 to +2.5 V and, in accordance with the experimental measurements, varies as a piecewise increasing and decreasing linear function with a slope of ±50 mV s^{-1}. The current in the I_{ds}–V_{ds} characteristic is given by the concurrent contributions of drift and diffusion components both in the surface native oxide (I_{drift}^{ox}, I_{diff}^{ox}) and in the bulk of the nanowire (I_{drift}^{NW}, I_{diff}^{NW}), and of the effects at the junctions (I_{SB1}, I_{SB1}). The implementation of the system required the estimations of different physical parameters for modeling the different components of the
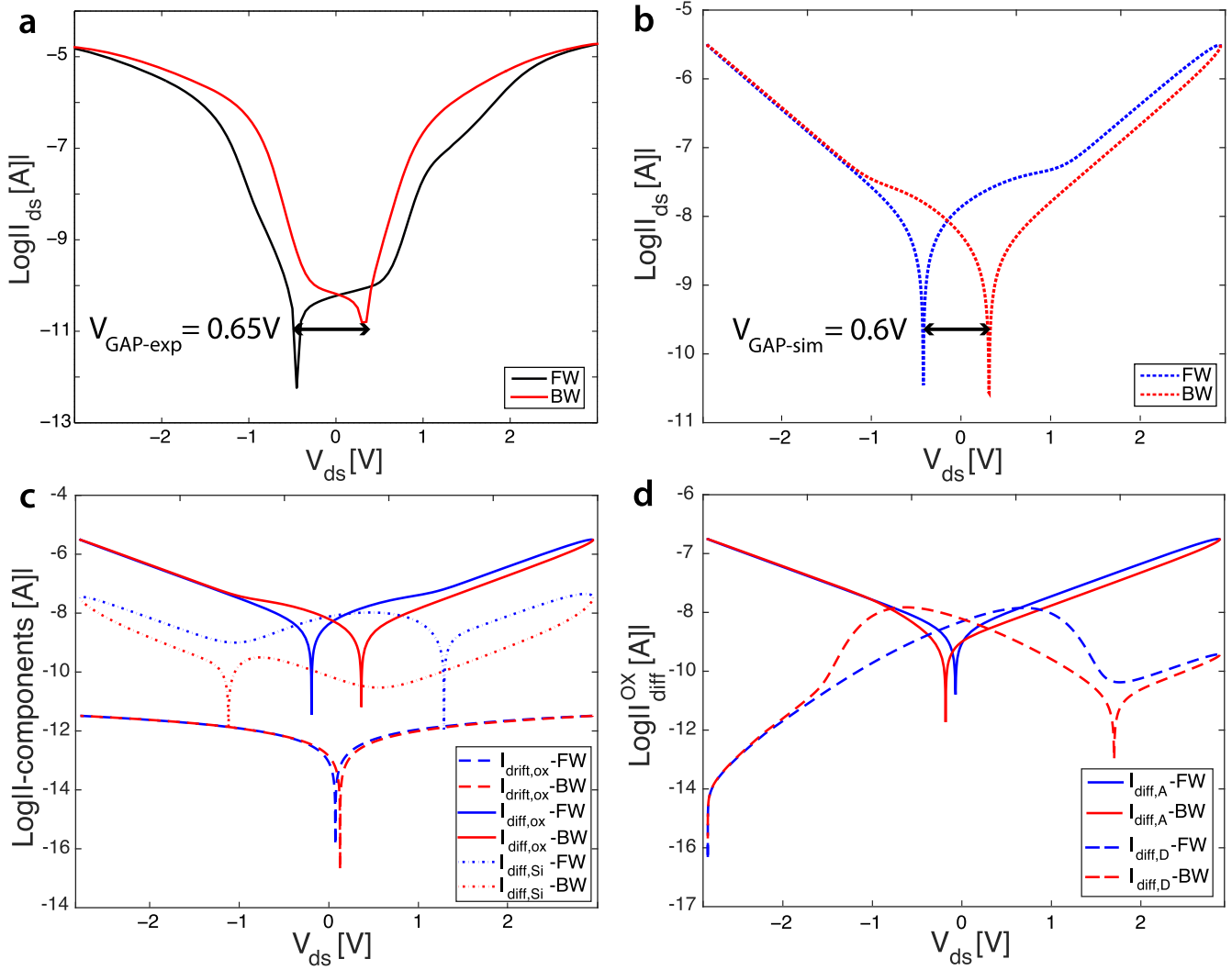
Figure 7. Modeling the voltage gap. (a) Semi-logarithmic I_{ds}–V_{ds} characteristic from experimental measurements acquired from a fabricated SiNW functionalized with ABs. The voltage gap appears as a result of the adsorption of positively charged species onto the nanowire and the interaction with the oxide surface states. (b) Simulated total I_{ds}–V_{ds} curve. (c) Components of the characteristic reported in panel (b): diffusion current due to the surface states in the oxide (solid curve); drift current in the oxide (dashed curve); diffusion current in the SiNW (dotted curve). (d) Individual contributions of acceptor (solid curve), and donor (dashed curve) states to the diffusive current at the NW surface. The parameters chosen for this simulation are: $k_{a0}^a = 3.5 \times 10^{-5}$ Hz, $k_{n0}^a = k_{a0}^a/[14(N_0 - n_{d,0})/n_{d,0}]$, $k_{n0}^d = k_{n0}^{d,BARE} \times 10^4$, $k_{d0}^d = (N_0 - n_{d,0})/n_{d,0} \times k_{n0}^d$, $\tilde{C}_a \sim \tilde{C}_d = 10^{-12}$ F, $\sigma = 6.5$, $\beta_a = \beta_d = 1/2$, $f_a = 2.8 \times 10^{14}$, $f_d = 3 \times 10^{14}$, $f_s = 2 \times 10^{16}$, $\Delta E = 253$ eV, $n_{d,0} = 0.69$, $N_0 \approx 40$.

current, as well as the fitting of some of them to the experimental data.

First, we considered the case of bare nanodevices, and we compared a real I_{ds}–V_{ds} measurement acquired from a SiNW after the fabrication and before any modification with biological material (figure 6(a)) with a simulated characteristic (figure 6(b)). As clearly evident from the plots, the simulated curve fits well the experimental one and models pinched hysteretic behavior (figure 6(b)). Figure 6(c) illustrates the corresponding components of the total current calculated in the simulation, components that are strictly dependent on each other and that affect the total current with their continuous competition/compensation. In the diagram, both forward and backward branches of the current are shown in order to better demonstrate the similarities between the

experimental and modeled curves under external voltage sweep.

The current $I_{drift}^{ox} + I_{diff}^{ox}$ arises from the dynamic exchange of charges at the surface trap states. The drift current in the surface oxide depends on the capacitances and resistances of the surface states in the oxide. C_α and R_α affect the total current because their product is comparable to the time of the system. Their effect varies as a function of the charge density n_α as a result of their definition (equations (2) and (3)).

Considering that the mobility of negative carriers, related to the acceptor states, is much higher than the one of positive carriers from donor centers ($\mu_a \approx 20$–30 cm^2 V^{-1} s^{-1}, $\mu_d \approx 10^{-5}$ cm^2 V^{-1} s^{-1} in p-doped silicon [42–44]), we observe that only the acceptor component contributes to the

drift transport being $R_a = 10^3$ MΩ, much smaller than $R_d = 10^6$ MΩ as estimated by equation (3). However, because of the high resistances of the surface trap networks in bare condition, the diffusion I_{diff}^{ox} related to the occupation of the acceptor and donor energy levels dominates (over I_{drift}^{ox}) the electrical transport at the surface (figure 6(c)).

The energy level related to the negatively charged acceptor states n_a is estimated [35] to be $|E_n^a| = 0.85$ eV, while the one corresponding to the positively charged donor states n_d is estimated [35] to be $|E_n^d| = 0.25$ eV. Consequently, the threshold energy associated with the neutral state is $|E_a^a| = E_i - 0.85$ eV for acceptors and $|E_d^d| = E_i - 0.25$ eV for donors, respectively, E_i being the intrinsic energy level of the semiconductor. The terms f_a and f_d in equation (5) are fitted to the experiments via Monte-Carlo simulations. Both in the bare and biomodified case they appear to be large ($f_a = 2.8 \times 10^{14}$, $f_d = 3 \times 10^{10}$ in the simulation curve of figure 6(b)). This indicates very small variation between the incoming and outgoing diffusion currents through the left and right surfaces of the SiNW, respectively (see section III of the SI). The diffusion current is plotted with solid curve in figure 6(c), and, as clearly visible in the figure, by looking at the amplitude of this component compared to the total curve of figure 6(b), it has the most important role in defining the pinched hysteresis loop in bare nanowires.

A further contribution may also come from the electronic transport in the bulk of the SiNW. However, both drift and diffusion currents in the nanowire core seem to be negligible in the condition in which external charged molecules are absent. I_{drift}^{NW} is not reported in figure 6(c) because of its very low amplitude. The low current values result from the fact that the nanowire channel can be approximated with a fully depleted channel as a consequence of the NiSi Schottky barriers, at both ends, defining depletion regions with thickness $w_{d1} \approx w_{d2} > L/2$. The depletion in the channel increases the resistance R_{Si} and makes the drift current of the bulk I_{drift}^{NW} negligible. Therefore, most of the current contributing to the transport in the SiNW core is given by the diffusion of carriers in the depleted regions (dotted curve in figure 6(c)).

The conductivity both in the nanowire and in the oxide is finally affected by the Schottky barriers (equation (10)), whose height has been estimated to be $\phi_{bi} \sim 0.45$ V [45]. No or little barrier lowering occurs in the absence of biomolecules. The junctions determine a small voltage drop at the NW contacts that limits the amplitude of the I_{ds}–V_{ds} characteristics of the device if compared to the biomodified condition that will be discussed in the following (figure 7). Most importantly, the condition of zero, or very small voltage gap, is directly related to the null quantity of acceptor states n_a and the low number of positively charged donor states n_d with respect to the total number of surface defects N_0 onto the native oxide. This value ($n_d/N_0 = 0.6$) demonstrates the balance of charges at the surface of the nanowire (neutral surface states) and the existence of few charged donor states mostly deriving from the doping atoms in the p-type semiconductor.

Figure 7 shows the nanowire behavior once exposed to charged molecules. Again, both forward and backward sweeps are highlighted. In figure 7(a), the I_{ds}–V_{ds} curve acquired from one memristive biosensor, i.e. a SiNW functionalized with ABs, which are positively charged species at physiological pH [46], are plotted. The biomodification determines the increase of the current maxima (two orders of magnitude bigger than the bare case (figure 6)) and, most relevantly, the appearance of a voltage gap defined by the different values acquired by forward and backward curves for the zero-current condition. Figure 7(b) is the plot of the simulated I_{ds}–V_{ds} curve.

Similar to the experimental curve, simulations show an increased current peak ($\sim 10^{-5}$ A) and a voltage gap of ≈ 1 V. The total simulated current in the SiNW is given by the sum of the different contributions (figure 7(c)) arising from the drift (dashed curve) and diffusion (dotted curve) current in the surface state network, and the diffusion in the nanowire channel (dotted curve), and is also dependent on the effects at the junctions. In addition, in this case, I_{drift}^{NW} can be neglected because of the fully depleted wire. As shown in figure 7(c), the predominant effect is given by the dynamic surface exchange of the energy levels, i.e. the diffusion in the oxide. This component is the result of the competing action of donor and acceptor states described by $I_{diff,a}^{ox}$ and $I_{diff,d}^{ox}$, respectively, in figure 7(d). The two currents depend on the constant rates k_β^d and k_β^a whose values were of the same order of magnitude in the case of pinched-loop hysteresis, i.e. bare devices ($k_{\alpha,0}^a \sim k_{\alpha,0}^d \approx 10^{-4}$ Hz), but now differ by three to four orders of magnitude, one with respect to the other. In particular, the dynamics of the energetic donor levels has increased ($k_{\alpha,0}^d \approx 2$ Hz), thus demonstrating that biomolecules attached to the nanowire surface favor the occupation of the donor energy levels. This occurs in combination with the increased number of positively charged donor levels n_d. This can be physically explained by considering the approaching and the binding of positively charged biomolecules, the ABs, to the surface of the nanowires. In other words, the incoming proteins charge the surface by providing positive charges and determine the occupation of the energetic levels associated with the donor defects. Negatively charged n_a do not interact with the external positive charges and cannot compensate for them, because of their null density at zero bias and in the initial condition of bare surfaces. However, with the adsorption of ABs, the formed biolayer may lead to the creation of new surface defects. These surface defects can be associated with acceptor energy levels, thus explaining the slowly increasing dynamics exchange for the acceptor-like surface states ($k_{\beta,0}^{a,BIO} \sim 10^4 k_{\beta,0}^{a,BARE}$). This is also confirmed by the increase of total number of surface traps N_0 in the curve simulating the voltage gap change after biofunctionalization ($N_0^{BIO} \approx 10 N_0^{BARE}$).

The surface trap capacitances $\tilde{C}_a$ and $\tilde{C}_d$ increase by two/three orders of magnitude with respect to the simulation of figure 6(b), due to the accumulation of a biolayer onto the device surface. However, these capacitances still do not affect in a relevant way the drift current in the oxide because of the low frequency of the biasing signal (order of mHz).
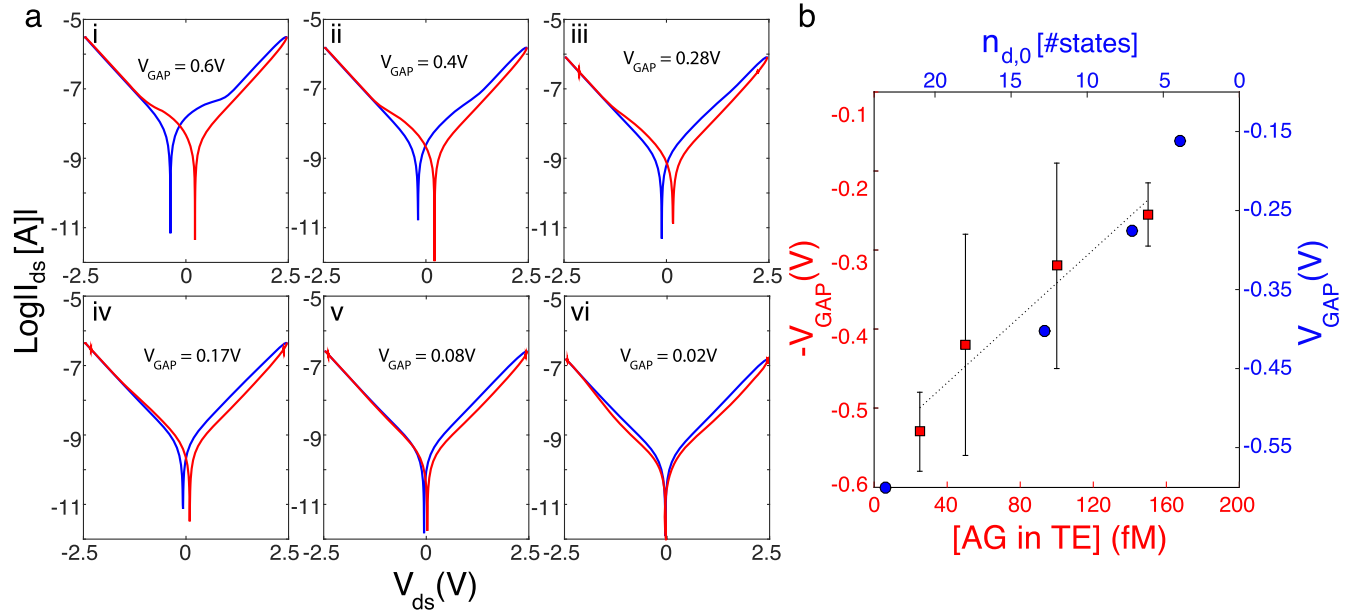
Figure 8. (a) Simulated I_{ds}–V_{ds} characteristics modeling the increasing uptake of AG molecules onto a biomodified nanowire. The parameters chosen in these simulations are: $\sigma = 6.5$, $\beta_a = \beta_d = 1/2$, $\tilde{C}_a \sim \tilde{C}_d = 10^{-12}$ F, $\Delta E = 253$ eV, $f_a = 2.8 \times 10^{14}$, $f_d = 3 \times 10^{10}$, $f_s = 2.5 \times 10^{15}$. Only some of the parameters in the model vary affecting the hysteresis and the voltage gap, demonstrating the importance of the charge imbalance induced by the dynamic modification of the surface states. Moving from plot (i) to plot (vi), $n_{d,0}$ decreases from 0.5 to 0.07, N_0 decreases from 47 to 8.4, and the donor rate constant k_{n0}^d decreases exponentially from $k_{n0}^d = 10^4 k_{n0}^{d,\text{BARE}}$ (i) to four orders of magnitude smaller in case (vi). (b) Reports the variation of the voltage gap as a function of $n_{d,0}$ (blue axes) and compares it to the calibration data from experiments (figure 3(b)) in a breast TE (red axes). As the AG concentration increases the positively charged surface states decrease due to charge compensation, thus determining a reduction of the voltage gap.

Thanks to its high dependence on external charges coming from the surrounding environment, the voltage gap can be used as biosensing parameter. The application proposed in this paper is the detection of AG molecules in a very challenging environment, which is a breast TE (figure 3(c)). As briefly explained above, the biosensing is determined by the electrical measurement of the voltage gap decrease from nanowire, which has been previously functionalized with ABs, namely the memristive biosensors, and successively exposed to increasing concentrations of target species. According to the theory proposed in this paper, the reduction of the voltage gap in the I_{ds}–V_{ds} characteristics is related to the charge compensation at the surface of the wire, where surface defects can easily become sites of charge accumulation under external sweeping bias and exposure to proteins. In figure 8 we demonstrate that our theory can model this dependence of the voltage gap on the increasing concentration of AGs, by correlating it to the formation and recombination of the charged surface states in the oxide of the SiNW.

The subplots in figure 8(a) give, from left to right and from top to bottom, simulated semi-logarithmic curves modeling the fabricated biosensor from the case of zero AG to the one of uptake of increasing concentrations. According to the surface trap mediated theory, the reduction of the voltage gap, combined with the lowering of the current peak, occurs as a result of different varying factors that have been observed from the simulation of the system. In general, they are related to variation in the surface states and their dynamics. Considering a linear variation of the AG concentration from the

case of figure 7, where the NW only carries positively charged ABs on its surface (0 fM) to the extreme case of AG concentrations saturating the sensor and determining a reduction of the voltage gap (figure 8(a), case (vi)) back to the starting pinched hysteresis loop (figure 6), the parameter $n_{d,0}$ decreases from 0.5 to 0.07, the parameter N_0 decreases from 47 to 8.4, and the donor rate constant k_{n0}^d decreases exponentially from $k_{n0}^d = 10^4 k_{n0}^{d,\text{BARE}}$ (i) to four orders of magnitude smaller in case (vi). The variation of the voltage gap as a function of $n_{d,0}$ is reported in figure 8(b) (blue axes) and superimposed to the experimental data (red axes) of figure 3(c) for comparison. This diagram demonstrates that the simulated results describe well the registered behavior of the voltage gap in real experiments of AG sensing in breast TEs, the first time reported for memristive biosensors, and explains the relationship between the sensing parameter and the decreasing number of positive surface states ($n_{d,0}$) on the wire as effects of increased concentration of AG and the occurrence of AB/AG binding phenomena resulting in charge compensation.

5. Conclusions

In conclusion, we have shown that the voltage gap sensing phenomenon in memristive biosensors is modeled by several combined effects of charge transport occurring at the nanowire surface; inside the wire and at the NiSi junctions. Despite the single phenomenon occurring in the sensor being relevant

to the determination of the memristive behavior of the device, and its modification in terms of voltage gap appearance, the major contribution comes from the dynamic occupations of the nanowire surface state energy bands, enabled by the incoming external charges from bio-species. This shows the importance of surface electrical transport in the oxide of the functionalized device.

We have presented the implementation of an analytical model able to reproduce and explain the voltage gap based behavior in NiSi Schottky barrier memristive biosensors, which successfully accounts for the detection of different concentrations of biomarkers for breast tumor screening. Moreover, the developed theory enables the capture of the dynamics of the voltage gap by using only a small set of parameters that are linked to the concentrations of antigens, thus enabling a determination of the number of antigens. Taking into account the direct correlation with the physics of the nanodevice, and the compactness of the model, our theory can be also used to model and predict the voltage gap based behavior in other similar nanostructured devices and sensors. This may be useful for several different applications ranging from biological and chemical sensing to electronics.

Acknowledgments

References

[1] Pandraud G, de Smet L C P M, Sudhölter E J R, Huang Q-A, Moh T S Y, Nie M and Sarro P M 2013 Effect of silicon nanowire etching on signal-to-noise ratio of SiNW FETs for (bio)sensor applications *Electron. Lett.* **49** 782–4

[2] Yates J T Jr 1991 Surface chemistry of silicon-the behaviour of dangling bonds *J. Phys.: Condens. Matter* **3** S143–56

[3] Bardeen J 1947 Surface states and rectification at a metal semi-conductor contact *J. Phys.: Condens. Matter* **71** 717–27

[4] Vermesh O, Wang O, Li Y M, Kim W, Javey A and Dai H J 2003 Hysteresis caused by water molecules in carbon nanotube field-effect transistors *Nano Lett.* **3** 193–8

[5] Effenberger F, Klauk H, Burghard M, Weitz R T, Zschieschang U and Kern K 2007 High-performance carbon nanotube field effect transistors with a thin gate dielectric based on a self-assembled monolayer *Nano Letters* **7** 22–7

[6] Kim T, Kim J, Alam M A, Jin S H, Islam A E and Rogers J A 2012 Sources of hysteresis in carbon nanotube field-effect transistors and their elimination via methylsiloxane encapsulants and optimized growth procedures *Adv. Functional Mat.* **22** 2276–84

[7] Paska Y and Haick H 2012 Interactive effect of hysteresis and surface chemistry on gated silicon nanowire gas sensors *ACS Appl. Mat. Inter.* **4** 2604–17

[8] Hanrath T and Korgel B A 2005 Influence of surface states on electron transport through intrinsic ge nanowires *J. Phys. Chem.* B **109** 5518–24

[9] Doucey M-A, Sacchetto D, Baj-Rossi C, Leblebici -Y, De Micheli G, Puppo F, Dave A and Carrara S 2014 Memristive biosensors under varying humidity conditions *IEEE Trans. Nanobiosci.* **13** 19–30

[10] Chua L 1971 Memristor-the missing circuit element *IEEE Trans. Circuit Theory CT-* **18** 579–519

[11] Chua L and Kang S M 1976 Memristive devices and systems *Proc. IEEE* **64** 209–23

[12] Di Ventra M and Pershin Y V 2013 On the physical properties of memristive, memcapacitive and meminductive systems *Nanotechnology* **24** 255201

[13] Doucey M-A, Baj-Rossi C, De Micheli G, Carrara S, Sacchetto D and Leblebici Y 2012 Memristive-biosensors: A new detection method by using nanofabricated memristors *Sens. Actuators B: Chem.* **171** 449–57

[14] De Micheli G, Puppo F, Di Ventra M and Carrara S 2014 Memristive sensors for pH measure in dry conditions *Surf. Sci. J.* **624** 76–9

[15] Patolsky F and Lieber C M 2005 Nanowire nanosensors *Mat. Today* **8** 20–8

[16] Curreli M, Zhang R, Ishikawa F N, Chang H K, Cote R J, Zhou C and Thompson M E 2008 Real-time, label-free detection of biological entities using nanowire-based FETs *IEEE Trans. Nanotechnol.* **7** 651–67

[17] Cui Y, Wei Q, Park H and Lieber C M 2001 Nanowire nanosensors for highly sensitive and selective detection of biological and chemical species *Science* **293** 1289–92

[18] Kim A, Ah C S, Yu H Y, Yang J-H, Baek I-B, Ahn C-G, Park C-W, Jun M S and Lee S 2007 Ultrasensitive, label-free and real-time immunodetection using silicon field-effect transistors *Appl. Phys. Lett.* **91** 103901

[19] Stern E, Klemic J F, Routenberg D A, Wyrembak P N, Turner-Evans D B, Hamilton A D, LaVan D A, Fahmy T M and Reed M A 2007 Label-free immunodetection with cmos-compatible semiconducting nanowires *Nature* **445** 519–22

[20] Chen K-I, Li B-R and Chen Y-T 2011 Silicon nanowire field-effect transistor-based biosensors for biomedical diagnosis and cellular recording investigation *Nano Today* **6** 131–54

[21] Rajan N K, Duan X and Reed M A 2013 Performance limitations for nanowire/nanoribbon biosensors *Wiley Interdisciplinary Reviews: Nanomedicine and Nanobiotechnology* **5** 629–45

[22] Pevzner A, Engel Y, Burstein L, Khatchtourints A, Lichtenstein A, Kantaev R, Elnathan R, Kwiat M and Patolsky F 2012 Biorecognition layer engineering: overcoming screening limitations of nanowire-based fet devices *Nano Lett.* **12** 5245–54

[23] Puppo F, Doucey M-A, Delaloye J-F, Moh T S Y, Pandraud G, Sarro P M, De Micheli G and Carrara S 2016 SiNW-FET in air biosensors for high sensitive and specific detection in breast tumor extract *IEEE Sens. J.* **16** 3374–3381

[24] Stern E, Wagner R, Sigworth F J, Fahmy T M, Breaker R and Reed M A 2007 Importance of the debye screening length on nanowire field effect transistor sensors *Nano Lett.* **7** 3405–9

[25] Knopfmacher O, Tarasov A, Fu W, Wipf M, Niesen B, Calame M and Schönenberger C 2010 Nernst limit in dual-gated si-nanowire fet sensors *Nano Lett.* **10** 2268–74

[26] Lee H G, Kim H J D and Kang S 2007 Single-protein molecular interactions on polymer-modified glass substrates for nanoarray chip application using dual-color tirfm *Bull. Korean Chem. Soc.* **28** 783–90

[27] Henderson L O, Whitfield -W, Vogt R F Jr., Phillips D L and Spierto F W 1987 Quantitative differences among various proteins as blocking agents for elisa microtiter plates *J. Immunological Methods* **101** 43–50

[28] He J, Zhu J, Gong C, Qi J, Xiao H, Jiang B and Zhao Y 2016 Label-free direct detection of miRNAs with poly-silicon nanowire biosensors *PLoS ONE* **10** 1–0 12

[29] Sacchetto D, Ben-Jamaa M H, Carrara S, De Micheli G and Leblebici Y 2010 Memristive devices fabricated with silicon nanowire schottky barrier transistors *Proc. 2010 IEEE Int. Symp. Circuits and Systems* pp 9–12

[30] Puppo F, Doucey M A, Moh T S Y, Pandraud G, Sarro P M, De Micheli G and Carrara S 2013 Femto-molar sensitive field effect transistor biosensors based on silicon nanowires and antibodies *SENSORS IEEE 2013, Baltimore, MD* pp 1–4

[31] Doucey M-A, De Micheli G, Tzouvadaki I, Puppo F and Carrara S 2015 Computational study on the electrical behavior of silicon nanowire memristive biosensors *IEEE Sens. J.* **15** 6208–17

[32] Zervas M, Carrara S, De Micheli G, Sacchetto D, Gaillardon P-E and Leblebici Y 2013 Applications of multi-terminal memristive devices: a review *IEEE Circuits Syst. Mag.* **13** 23–41

[33] Schroder K and Babcock J A 2003 Negative bias temperature instability: road to cross in deep submicron silicon semiconductor manufacturing *Appl. Phys. Rev.: D* **94** 1–8

[34] Achuthan M K and Bhat K N 2007 *Fundamentals of Semiconductor Devices* (New Delhi, India: Tata McGraw-Hill)

[35] Ragnarsson L-A and Lundgren P 2000 Electrical characterization of P_b centers in (100)Si-SiO$_2$ structures: the influence of surface potential on passivation during post metallization anneal *J. Appl. Phys.* **88** 938–42

[36] Gray P V and Brown D M 1966 Density of SiO$_2$-Si Interface States *Appl. Phys. Lett.* **8** 31–3

[37] Sze S M and Ng K K 2007 *Physics of Semicondutor Devices* 3rd Edn (New York: Wiley)

[38] Rhoderick E H and Williams R H 1988 *Metal-Semiconductor Contacts* (Oxford, USA: Claredon Press)

[39] Chu H-L *et al* 2014 Density of SiO$_2$-Si Interface States *Nano Lett.* **14** 1026–31

[40] Zwolak M, Wilson J and Ventra M Di 2010 Dehydration and ionic conductance quantization in nanopores *J. Phys.: Condens. Matter* **22** 454126

[41] Tang A Y, Drakinskiy V, Yhland K, Stenarson J, Bryllert T and Stake J 2013 Analytical extraction of a schottky diode model from broadband S-parameters *IEEE Trans. Microw. Theory Technol.* **61** 1870–8

[42] Goodman A M 1976 Electron Hall effect in silicon dioxide *Phys. Rev.* **164** 1145–115

[43] Hughes R C 1975 Hole mobility and transport in thin SiO$_2$ films *Appl. Phys. Lett.* **26** 436–8

[44] Pecht M, Radojcic R and Rao G 1998 *Guidebook for Managing Silicon Chip Reliability* (Boca Raton, Florida: CRC Press LLC)

[45] De Marchi M, Sacchetto D, Frache S, Zhang J, Gaillardon P, Leblebici Y and De Micheli G 2012 Polarity control in double-gate, gate-all-around vertically stacked silicon nanowire fets *2012 IEEE Int. Conf. on Electron Devices Meeting (IEDM)* pp 8.4.1–8.4.4

[46] Carrara S 2013 *Bio/CMOS Interfaces and Co-Design* (New York Heidelberg Dordrecht London: Springer)